HiSST: 3rd International Conference on
High-Speed Vehicle Science Technology
14 -19 April 2024, Busan, Korea

Aerodynamic and Propulsive Assessment of an Experimental Hypersonic Scramjet System

Pietro Roncioni[1], Oreste Russo[2], Francesco Cascone[3],
Marco Marini[4], Sara Di Benedetto[5], Marta Albano[6], Roberto Bertacin[7]

Abstract

The present paper deals with the aerodynamic and propulsive characterization of a Hypersonic Scramjet System, composed by Launch Vehicle (LV) and Flight Demonstrator (SHEV), as part of a research project on experimentation for hypersonic flight and enabling technologies for future high-speed transportation systems, co-funded by CIRA and ASI. The winged rocket-based launch vehicle is conceived to bring at target altitude and velocity the scramjet hypersonic experimental vehicle (SHEV) posing the challenge of creating, at national level, an aircraft capable of supporting a levelled hypersonic flight thanks to the introduction of a scramjet propulsion system.

Keywords: Scramjet, CFD, Hypersonic, Aerodynamic Database.

1. Introduction

The activities of the present paper are part of a research project aimed to develop, in the long term, a national hypersonic vehicle and related technologies by means of experimentation, in order to pave the way to future high-speed transportation systems. The project complements several initiatives born in Europe in the last 20 years: the various EU projects dedicated to hypersonic passenger flight (LAPCAT I&II, ATLLAS I&II, FAST20XX, HIKARI, HEXAFLY, HEXAFLY-INT, STRATOFLY) and the national initiatives that led to the design of prototypes such as, among others, the ZEHST French aircraft, developed by MBDA, ASTRIUM and ONERA, or the English SKYLON by Reaction Engines Ltd., which despite being more oriented towards supersonic flight and access to space, respectively, already include many of the technologies necessary for hypersonic flight. Hypersonic civil transport has always had as its weak point the low cruising autonomy, essentially linked to too high fuel consumption. In recent years, a highly integrated design approach between efficient propulsion systems and high-lift configurations (LAPCAT-II and STRATOFLY configurations) is enabling the trend to be reversed ([1], [2], [3], [4]).

The study on the Scramjet Hypersonic Experimental Vehicle (SHEV) starts from the experience gained thanks to the strong involvement of Italian companies, and CIRA in particular, in the European project HEXAFLY-INT (realization of a flight test of an aircraft without engine for hypersonic flight), and previously in the HEXAFLY one, posing the challenge of creating an aircraft capable of supporting a levelled hypersonic flight thanks to the introduction of a scramjet propulsion system ([5], [6], [7]). The project is co-funded by the national research programme PRORA and the Italian Space Agency (ASI), with the aim of designing a hypersonic propelled demonstrator capable of performing a levelled and

[1] *CIRA, Italian Aerospace Research Centre, 81043 Capua, Italy, p.roncioni@cira.it*
[2] *CIRA, Italian Aerospace Research Centre, 81043 Capua, Italy, o.russo@cira.it*
[3] *CIRA, Italian Aerospace Research Centre, 81043 Capua, Italy, f.cascone@cira.it*
[4] *CIRA, Italian Aerospace Research Centre, 81043 Capua, Italy, m.marini@cira.it*
[5] *CIRA, Italian Aerospace Research Centre, 81043 Capua, Italy, s.dibenedetto@cira.it*
[6] *ASI, Agenzia Spaziale Italiana 00133 Rome, Italy, marta.albano@asi.it*
[7] *ASI, Agenzia Spaziale Italiana 00133 Rome, Italy, roberto.bertacin@asi.it*

controlled flight at Mach 6÷8 and an altitude of 28÷32 km, in order to realize and test in flight the enabling technologies for future civil transport systems at hypersonic speed.

This paper deals with activities that aim to verify the aerodynamic efficiency (L/D = 3÷4) and the aero-propulsive balance (T>D) at Mach = 6÷8 in controlled flight of the demonstrator, and the aerodynamic database of the full system composed by the launch vehicle and the above-mentioned demonstrator. In particular, the capability of the launch system to bring the demonstrator at the required altitude and velocity has to be verified in terms of stability, manoeuvrability and trimmability. Another important point is the safe releasing of the SHEV vehicle. For the purpose of verifying the above requirements numerical viscous CFD simulations were conducted for both the full system and the demonstrator in the experimental window in fuel-off and fuel-on conditions. For the SHEV, in particular, it is important to calculate the values of aerodynamic efficiency and mass flow of air at the combustor inlet, and the verification of the aero-propulsive balance (T>D) that requires the development of reacting Hydrogen-Air simulations.

2. Mission and System Description

The preliminary mission concept envisages an air-launched solution with a carrier (stage I) capable of releasing the payload, composed by the propelled hypersonic demonstrator and the launch vehicle equipped with a booster, at a target point in terms of speed and altitude. From here the launch vehicle accelerates until it reaches the foreseen trajectory target point in terms of Mach and altitude, where the hypersonic propelled demonstrator is released and the scramjet must work for a time of at least 10 seconds.

It is therefore possible to identify three mission phases (Figure 1): Step 0: from the release of the payload from the carrier to the release of the demonstrator at the target point (Sep1 and Sep2 of Fig 1, respectively); Step 1: Experimental window; Step 2: Gliding phase.

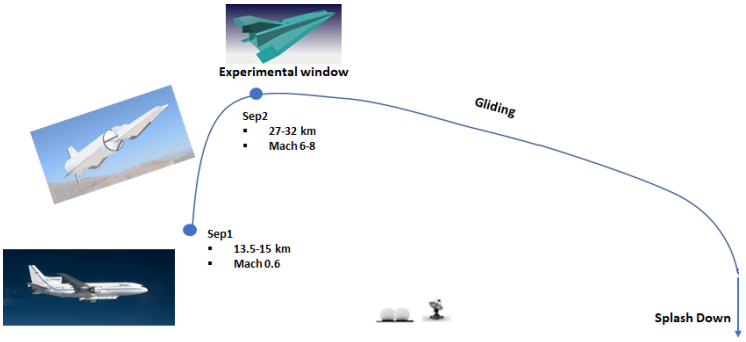

Figure 1: Mission Scenario.

The launch vehicle connected to the propelled hypersonic demonstrator is represented in Figure 2.

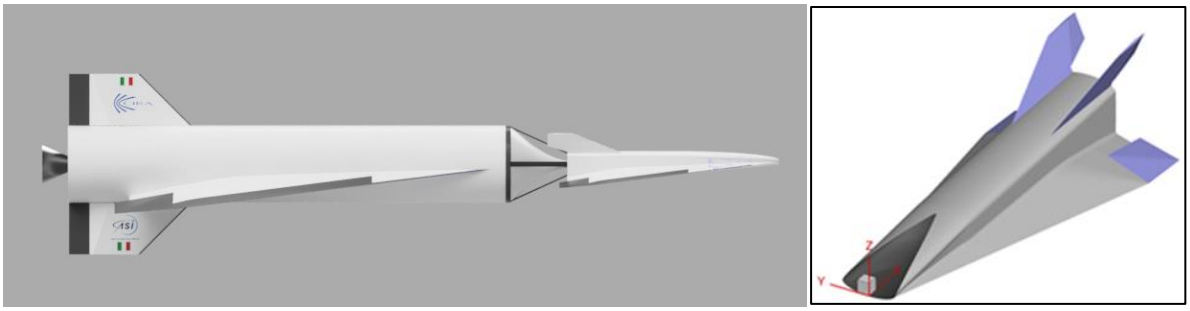

Figure 2. Full Launch System (left) and Demonstrator (right).

The configuration of the propelled hypersonic demonstrator is based on the concept of "waverider", or a hypersonic vehicle with high aerodynamic efficiency in supersonic regime obtained through the exploitation of shock waves that form on the lifting surfaces, a phenomenon known as "compression

lift". The demonstrator must also include a scramjet air-breathing propulsion system. The concept is depicted in Figure 3, and is an heritage of the already studied EU-FP7 HEXAFLY (see refs [5], [6], [7]).

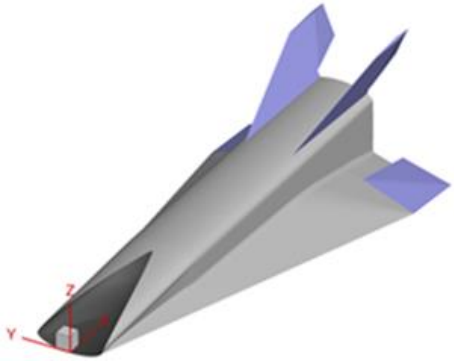

Figure 3: Configuration of the SHEV vehicle.

3. AEDB Building and Results

The AErodynamic Data Base (AEDB) building is the overall procedure that allows to obtain a full and integral set of information and/or data that characterize the aerodynamic environment in terms of flow field features, global and local forces and pressure distributions over the vehicle surfaces.
In particular, the main parameters to be defined are:

- Components of aerodynamic forces and moments versus the main variables characterizing the flight, i.e., Mach and Reynolds numbers, angle of attack, angle of sideslip, deflection of control surfaces, etc.
- Uncertainties levels to be added to the previous nominal data.
- Surface pressure distributions.

These data are inputs for several disciplines as flight mechanics, thermo-structural analysis, but also in some cases for propulsive database building.
The final and reliable aerodynamic database is foreseen to be obtained by means of both numerical and experimental activities. In this paper the starting activities results are reported, i.e.:

- Aero-propulsive Balance and Aerodynamic Efficiency assessment.
- Numerical aerodynamic database built by means of CFD simulations.

4. Aero-Propulsive Balance and Aerodynamic Efficiency

The verification of the aero-propulsive balance and aerodynamic efficiency in cruise conditions is presented in this paragraph. For this purpose, two flight conditions falling within the required Mach and altitude ranges were considered (see Table 1).

Table 1: Matrix test for hypersonic cruise conditions.

Altitude	H = 27 km	H = 31.9 km
Static pressure p_∞	1828 Pa	875.5 Pa
Static temperature T_∞	222.3 K	235.97 K
Static density ρ_∞	0.02852 kg/m3	0.01293 kg/m3
Mach number M_∞	7.350	7.355
Flow velocity u_∞	2202 m/s	2264.7 m/s
MFR	**4.851 kg/s**	**2.246 kg/s**

Numerical CFD viscous simulations were conducted by means of the ANSYS FLUENT® CFD code on a grid of 7.6 million cells (Figure 4) and with the thermal boundary conditions shown in Figure 5.

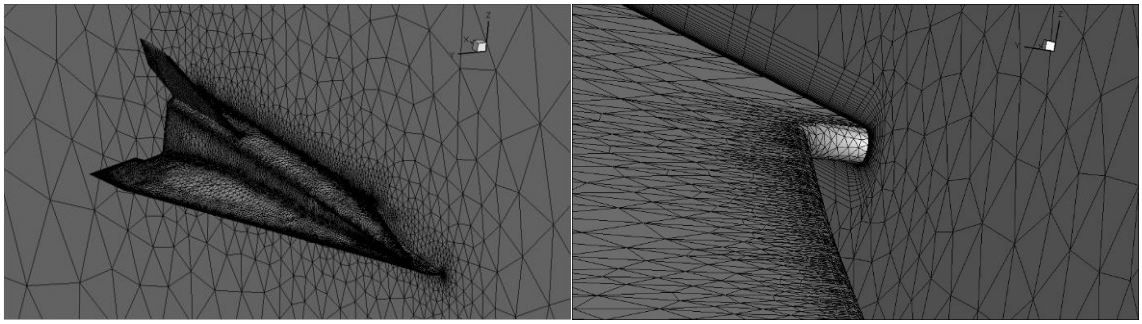

Figure 4: Computational grid for simulations with the engine on.

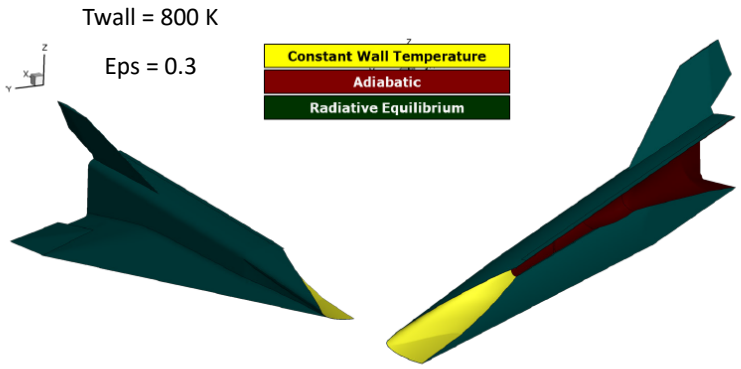

Figure 5: Applied thermal boundary conditions.

The initial simulations conducted with the engine off settings (Fuel-off) provided us with the values of vehicle's aerodynamic efficiency and mass flow of air at the combustor inlet. This last value served as input for the sizing of the tanks and fuel supply lines, an activity conducted by the propulsion unit.
Table 2 summarizes the aerodynamic parameters of interest. The values were extracted by distinguishing the external part (fuselage, wings and empennages) and the internal part composed of air intake, combustor and nozzle. The flight experiment takes place in motor-on conditions, and in these conditions for the purposes of aerodynamic efficiency estimation only the external part of the aircraft is considered, this is because the whole internal duct acts as an engine and has a positive thrust such as to balance the drag of the remaining part of the aircraft (external part). In such conditions the total drag is zero. From the table you can see how the efficiency E_{ext} (external) is well above 4 (almost 5). It will be seen later that this value is also confirmed in motor-on conditions.
In addition, from the table it is possible to see that even the total efficiency E_{tot}, which makes sense as argued above for the motor-off conditions that occur after the shutdown of the scramjet, is well within the mission requirements (value around 3.5).

Table 2: Summary of aerodynamic parameters of cruising with the engine off.

H	Mach	Type	CL_ext	CL_int	CL_tot	CD_ext	CD_int	CD_tot	CM_ext	CM_int	CM_tot	E_ext	E_int	E_tot
27.00	7.350	No-Inj	0.04004	0.001299	0.041339	0.008267	0.00336	0.01163	-0.02362	-0.00304	-0.02667	4.8431	0.3865	3.5552
31.90	7.355	No-Inj	0.03996	0.001166	0.041130	0.008604	0.00345	0.01205	-0.02355	-0.00296	-0.0265	4.6449	0.3380	3.4125

Following the verification of the aerodynamic efficiency requirement, it was then necessary to verify the aero-propulsive balance. This expression means that the thrust delivered by the scramjet engine must be verified to counterbalance the aerodynamic drag of the external part of the aircraft. Before this assessment it is necessary to verify that the balance of the internal path alone is first verified, that is, the engine starts and the gross thrust of the "thrust chamber" (combustor + nozzle) is at least able to overcome the drag of the intake (very high in hypersonic conditions). The net thrust, i.e., the gross thrust decreased by the drag of the air intake (which is considered to be part of the engine), must therefore be greater than or equal to the external drag.
Simulations with air-hydrogen reacting flow were therefore conducted under the same asymptotic conditions as in Table 1. For the fuel injection, two front semi-struts have been provided, positioned at the beginning of the combustion chamber and on both sides of the same, and a rear full-strut positioned further downstream and laying on the symmetry plane (see Figure 6). Each semi-strut is provided with

a single injection hole positioned on the top, whereas the full strut is equipped with four injection holes positioned on the sides and rear.

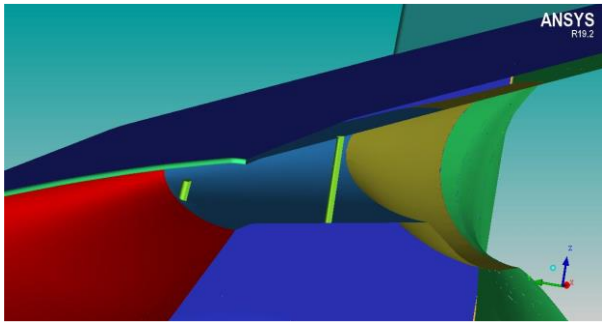

Figure 6: Positioning of semi-strut and strut in combustion chamber (half aircraft).

Starting from the mass flow data of air entering the combustion chamber, and setting the hydrogen-air equivalence ratio (ER: Equivalence Ratio), it is then possible to calculate the mass flow rate of hydrogen to be introduced into the chamber. In the present simulations an ER equal to 1 (stoichiometric proportions) was considered which corresponds to a ratio of hydrogen/air flow rates equal to 0.02924; this flow rate of H_2 was divided between semi-struts and full strut with the following ratios: 0.65 and 0.35, respectively. Table 3 reports the details of fuel injection.

Table 3: Fuel inlet parameters (half configuration).

H	Mach FF	MFR air	ER	MFR H2	M des	Struts	Ptot	Pexit	Mexit
[km]	[-]	[kg/sec]	[-]	[kg/sec]	[-]		[Pa]	[Pa]	[-]
27.00	7.350	2.4255585	1.00	0.0709233	2.00	semi (1)	5510165	704224	1.9927
					2.00	full (2)	9020220	1152825	3.0454
31.90	7.355	1.1227676	1.00	0.0328297	2.00	semi (1)	5643204	721227	2.0000
					2.00	full (2)	3490761	446135	2.0000

In order to not weigh down the numerical calculations too much, a single-step chemical scheme for modelling air-hydrogen combustion was used that considers the only reaction between oxygen and hydrogen, with nitrogen that remains inert and unchanged along the entire internal duct, according to the following scheme:

$$2H_2 + O_2 + 79/21\ N_2 \rightarrow 2H_2O + 79/21N_2$$

From which it is possible to derive stoichiometric mass ratios

$$\frac{\dot{m_{air}}}{\dot{m_{fuel}}} = \frac{\frac{79}{21} * 28 + 1 * 32}{2 * 2} = \frac{2884}{84} = 34.2;\ \frac{\dot{m_{fuel}}}{\dot{m_{air}}} = 0.02924$$

Below is reported also the definition of Equivalence Ratio:

$$\varphi = ER = \frac{\left(\frac{\dot{m_{fuel}}}{\dot{m_{air}}}\right)_{actual}}{\left(\frac{\dot{m_{fuel}}}{\dot{m_{air}}}\right)_{stoich}}$$

In the following figures (Figure 7 and Figure 8) you can see the temperature and water vapor distributions within the propulsive duct. It can be seen that the reaction takes place along the entire propulsive duct (combustion chamber + nozzle) leading to an increase of temperature. Due to the high temperature value, the water is in the gaseous state and, as also appears in Figure 8, is almost uniform in the nozzle region. One of the purposes of these simulations with single-step reaction is just to verify that combustion takes place satisfactorily.

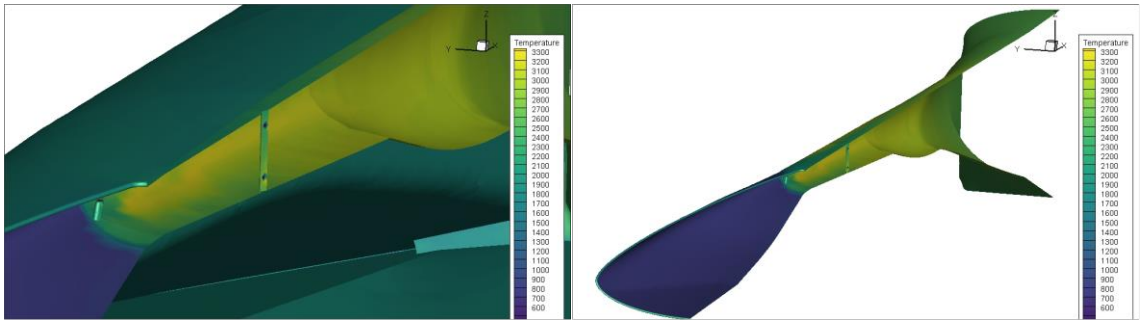

Figure 7: Temperature distributions on the inner walls of the propulsive duct.

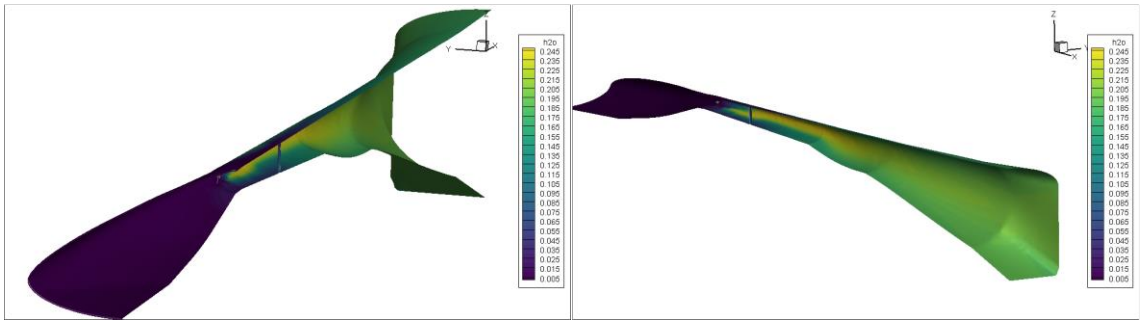

Figure 8: Distribution of water vapor inside the propulsion duct.

Table 4 shows the main results in terms of aerodynamic coefficients for both motor-off (already reported above) and motor-on conditions. First of all, it can be noted that the aero-propulsive balance requirement is met at both altitudes. In fact, the total drag CD_tot (external + internal) is negative, which means that the thrust of the scramjet engine (C_{thrust} = -CD_{int}) is higher than the external drag (CD_{ext}). Also, from the same table it can be seen that the aerodynamic efficiency values (E_{ext}) remain essentially unchanged compared to the corresponding motor-off cases and largely satisfying the relative mission requirement. Finally, Table 5 shows the aero-propulsive balance in quantitative terms, too.

Table 4: Summary of aerodynamic parameters for cruising with both engine on and off.

H	Mach	Type	CL_ext	CL_int	CL_tot	CD_ext	CD_int	CD_tot	CM_ext	CM_int	CM_tot	E_ext	E_int	E_tot
27.00	7.350	React	0.04032	0.001298	0.041618	0.008509	-0.00915	-0.00064	-0.02380	-0.00295	-0.02675	4.7386	-0.1418	-64.8527
31.90	7.355	React	0.03885	0.002026	0.040875	0.008539	-0.00868	-0.00015	-0.02295	-0.00306	-0.02601	4.5498	-0.2334	-281.5156
27.00	7.350	No-Inj	0.04004	0.001299	0.041339	0.008267	0.00336	0.01163	-0.02362	-0.00304	-0.02667	4.8431	0.3865	3.5552
31.90	7.355	No-Inj	0.03996	0.001166	0.041130	0.008604	0.00345	0.01205	-0.02355	-0.00296	-0.0265	4.6449	0.3380	3.4125

Table 5: Summary of axial forces acting on the hypersonic propelled demonstrator.

		Ext	Int	Tot
Forces (N)	**27 km**	**2820**	**-3032**	**-213**
Mot-on	**31.9 km**	**1357**	**-1380**	**-23**
Forces (N)	**27 km**	**2740**	**1113**	**3853**
Mot-off	**31.9 km**	**1367**	**548**	**1915**

In order to verify the effect of the chemical kinetics modelling for air-hydrogen combustion, an additional analysis has been done by considering a simplified configuration of only the internal flow path (see Figure 9) and a more detailed chemical scheme for air-hydrogen combustion (i.e., Jachimowski with 9 species and 12 reactions).

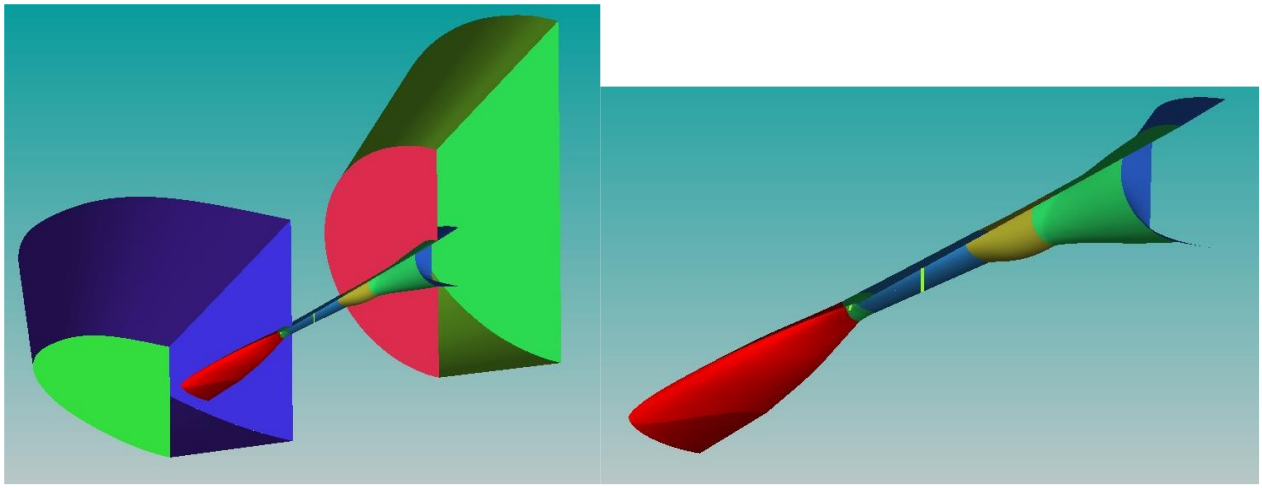

Figure 9: Internal flow path configuration.

Table 6: Summary of axial forces acting on the hypersonic propelled demonstrator.

	Domain	CD_intake	CD_struts	CD_comb_nozzle	CD_all_int	F_comb_nozzle	F all int
Mono-st	whole	0.005221652	0.00146725	-0.015839459	-0.009151	**-2624**	**-1516**
Mono-st	internal	0.003486158	0.00274239	-0.016867853	-0.010639	**-2795**	**-1763**
Jachi	internal	0.003509144	0.00264422	-0.015555827	-0.009402	**-2577**	**-1558**

Main results are reported in Table 6 and can be summarized as follows:

- Good comparison between whole domain (NS) and internal domain (EUL) for what concerns the net thrust (all internal flow path). 1516 vs 1763 N
- Reduction of about 11% of net thrust (all internal path) using a more detailed chemical scheme. 1763 N → 1558 N
- Reduction of about 8% of gross thrust (combustor and nozzle) using a more detailed chemical scheme. 2795 N → 2577 N.

The reduction of the thrust should be in any case compensated with using a higher ER (i.e., by injecting more fuel).

5. Aerodynamic Database

This section describes the operations performed in order to obtain the Aerodynamic Database (AEDB) for the hypersonic propelled demonstrator (Figure 3) which will be useful for conducting flight mechanics analyses ([8], [9], [10], [11], [12], [13]).
The aerodynamic database is provided as a function of Mach number (M_∞), angle of attack (α) and the elevon deflections (δ_e) in *fuel-off* conditions. However, the analysis does not consider the effect of sideslip angle (β). The reference quantities are reported in Table 7. The Centre of Gravity is located at x_{CoG} = 2.33 m from the nose.

Table 7: Summary: Reference Quantities.

Reference Length (L_{ref})	4.1248 m
Reference Surface (S_{ref})	4.7936 m^2
Mass	1120 kg
x_{CoG} range	2.30÷2.33 m

5.1. SHEV Clean Configuration

The aerodatabase of the SHEV vehicle has been completed from Mach 7.35 to Mach 2; indeed, the mission foresees, after the ignition time (at least 10 seconds at constant altitude), a gliding aerodynamically controlled phase followed by a splash down on the sea. The database will be then completed to cover the whole mission till splash down. The CFD computations have been obtained

running on the same grid of 7.6 million of cells and with the same turbulence model, but now in fuel-off conditions (see Table 8).
A sensitivity in fuel-on cruising conditions has been also performed by adding ±2deg to AoA=0 deg at M=7.35 while a range from -4° to +4° for the AoA in fuel-off ones has been considered. The fuel-off descent, based on the estimated preliminary trajectory, needs to be verified at a later stage in the analysis of Flight-Mechanics. The AEDB data is released with increasing reliability for flight mechanics analysis and trajectory calculation in the framework of the project.

Table 8: Test Matrix for CFD computations.

h (km)	Mach	AoA	engine	P	Temp	Dens	a	Vel	mu
27.00	7.35	-2, 0, 2, 4	fuel-off/on	1847.46	223.65	0.028777	299.799	2203.52	1.47164E-05
26.19	7	-2, 0, 2, 4	fuel-off	2091.26	222.84	0.032693	299.255	2094.79	1.46711E-05
25.25	6	-2, 0, 2, 4	fuel-off	2416.16	221.90	0.037932	298.623	1791.74	1.46324E-05
23.36	5	-2, 0, 2, 4	fuel-off	3236.22	220.01	0.051243	297.349	1486.75	1.45123E-05
20.54	3.5	-2, 0, 2, 4	fuel-off	5028.52	217.19	0.080656	295.437	1034.03	1.43532E-05
17.72	2	-2, 0, 2, 4	fuel-off	7843.63	216.65	0.126124	295.070	590.14	1.43226E-05

Looking at the following figures (from Figure 10 to Figure 12) we can deduce that:

- A linear trend of CL is predicted for full vehicle (External + Internal) except in fuel-on conditions (M=7.35) where there is a decrease of the derivative CL_α with increasing of AoA.
- A quadratic trend of CD is predicted. At M=7.35 fuel-on the aero-propulsive balance is "negative" at AoA=2° that means that the external drag is greater than the "net thrust" of the internal flow path. This is due to the fact that at higher angle of attack the intake captures less air (massflow spillage) and so the scramjet engine produces a lower "thrust". The opposite can be observed at AoA=-2° where there is a higher massflow rate and thrust.
- In the gliding phase from M=7.35 to M=2.0 an out of trend of CL can be observed (see Figure 12). At M=3.5 the CL is lower than expected. This is due to the expulsion of the shock waves train from combustor duct, and the consequent positioning of a nearly normal shock wave over the intake giving a local down-lift (intake hysteresis phenomenon).
- The external aerodynamic coefficients are all regular as expected from linear aerodynamics. There is no influence of the shock wave train positioning along the gliding trajectory.
- From the internal coefficients we can see, as expected from previous considerations, great values of drag and down-lift at M=2.0, 3.5 (expulsion of shock waves train), small values for other Mach numbers and in particular negative drag (that means positive internal thrust) at M=7.35 fuel-on conditions.

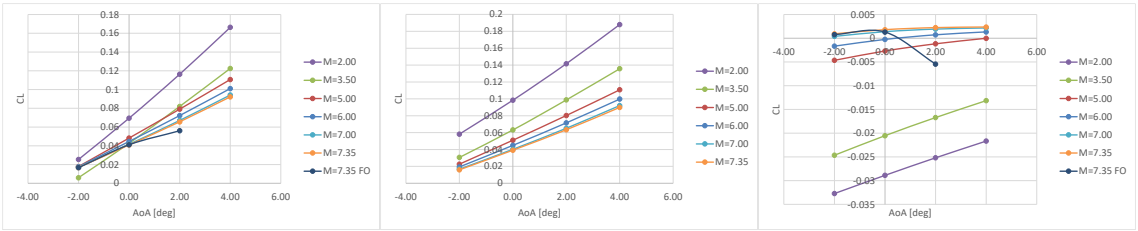

Figure 10: Lift Coefficient: Full vehicle, External part, Internal part.

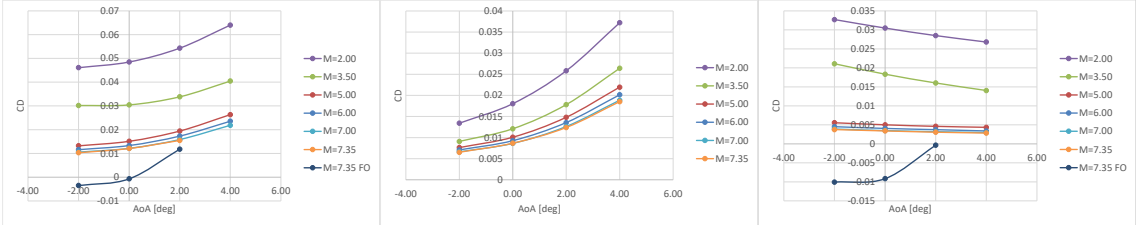

Figure 11: Drag Coefficient: Full vehicle, External part, Internal part.

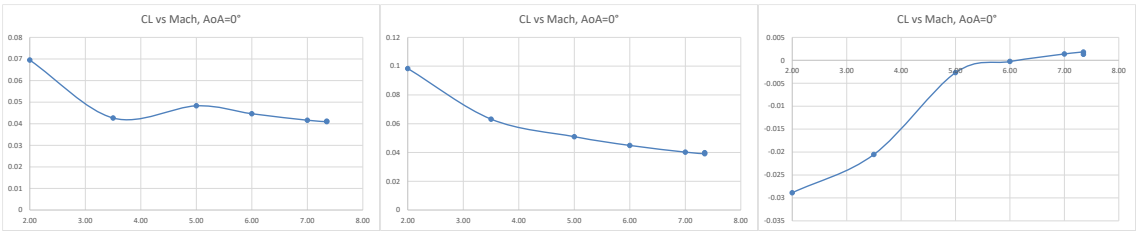

Figure 12: Lift Coefficient at AoA=0°: Full vehicle, External part, Internal part.

5.2. SHEV Control Surfaces Effect

The SHEV aerodatabase with considering the deflection of control surfaces (i.e., the elevons) is reported in this section. The variation of the aerodynamic coefficients is assessed as the difference between the aerodynamic coefficients of the configuration evaluated with deflected elevon and the coefficients evaluated with the undeflected elevon, i.e., considering the pitching moment coefficient as an example:

$$\Delta \boldsymbol{C_M}(\boldsymbol{\delta_e}) = C_{M_{\delta_e}} - C_{M_{\delta_e=0}}$$

In order to calculate data for elevon's effect a simplified configuration constituted by the wing and elevon has been considered (Figure 13), and CFD simulations have been performed with the inviscid flow hypothesis.
The following ranges have been analysed to generate the longitudinal aerodynamic data sets:
• $2 \leq M_\infty \leq 7.35$
• $-2° \leq \alpha \leq 4°$
• $-20° \leq \delta_e \leq 10°$
The Pitching Moment Coefficient of the flapped wing is reported in Figure 14.

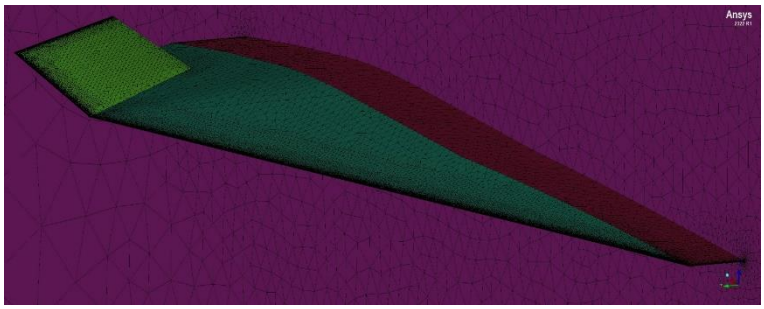

Figure 13: Grid for a stand-alone wing with a deflected elevon.

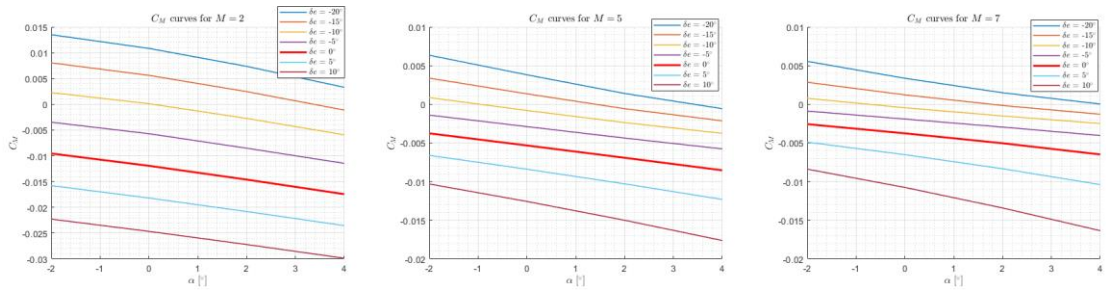

Figure 14: Effect of Flap Deflection on Pitching Moment Coefficient.

As a final step, the complete aerodynamic database is described, i.e., the database of the hypersonic propelled demonstrator configuration that considers also the effect of control surfaces (elevons). Figure 15, Figure 16 and Figure 17 show, respectively, the lift, drag and pitching moment coefficient distributions in function of AoA for three different elevon deflections (-20°, -5°, +10°) and Mach numbers (from 2.0 to 7.35).

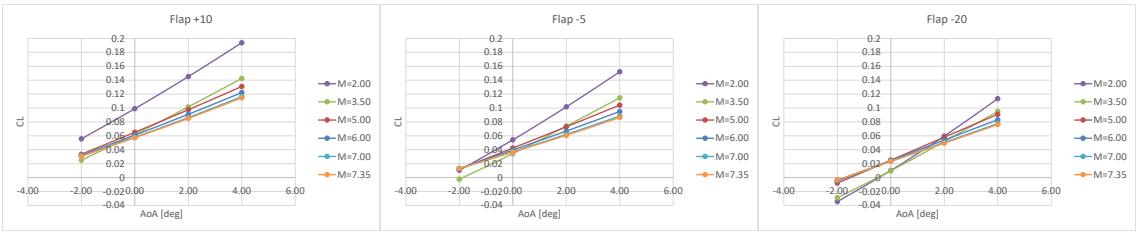

Figure 15: Lift Coefficient at three different elevon deflections.

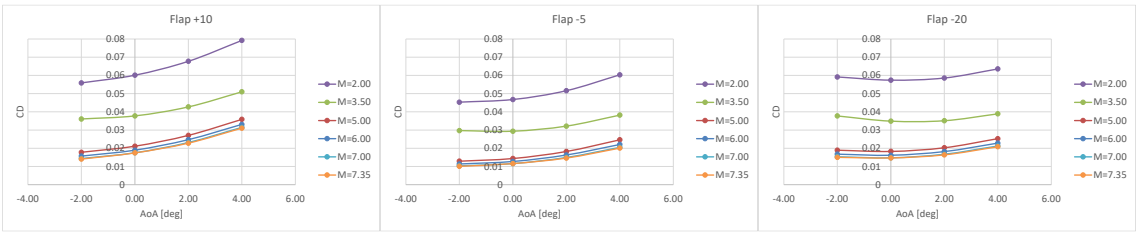

Figure 16: Drag Coefficient at three different elevon deflections.

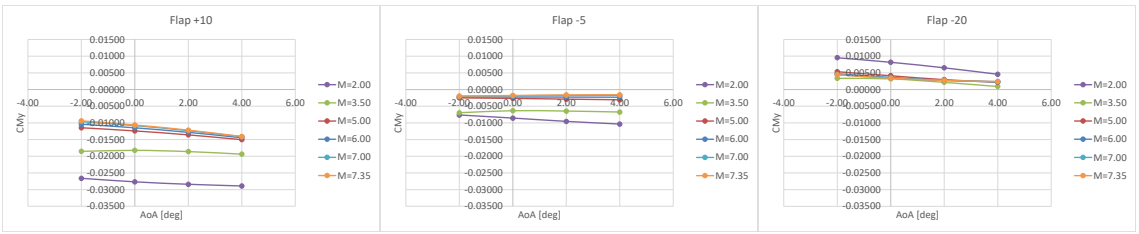

Figure 17: Pitching Moment Coefficient at three different elevon deflections.

5.3. Full Launch System

The calculation of the aerodynamic coefficients for the clean configuration of the full launch system (the scramjet hypersonic demonstrator coupled to the launch vehicle) has been obtained by means of inviscid CFD simulations. Those simulations are carried out with using the commercial code ANSYS FLUENT®. Each solution is assumed to be convergent when the residuals drop more than three orders of magnitude, and the aerodynamic coefficients reach a constant value.
The reference quantities considered for these calculations are the same already used for the SHEV, in order to obtain aerodynamic coefficients that are easily comparable with those already calculated on the demonstrator (Table 7).
The full AEDB has been evaluated on two different meshes for subsonic and supersonic conditions in order to respect the far field conditions in all the directions.
The computational grids have been generated using the ICEMCFD® software. The unstructured grids have about 7 million cells (for half configuration). In addition, an adaptive mesh based on a density gradient criterion was implemented in some regions, in order to capture the shock wave in the divergent nozzle of the SHEV when the asymptotic Mach number is not high enough, and the curved shock that forms on the shaped cone of the Launch Vehicle.

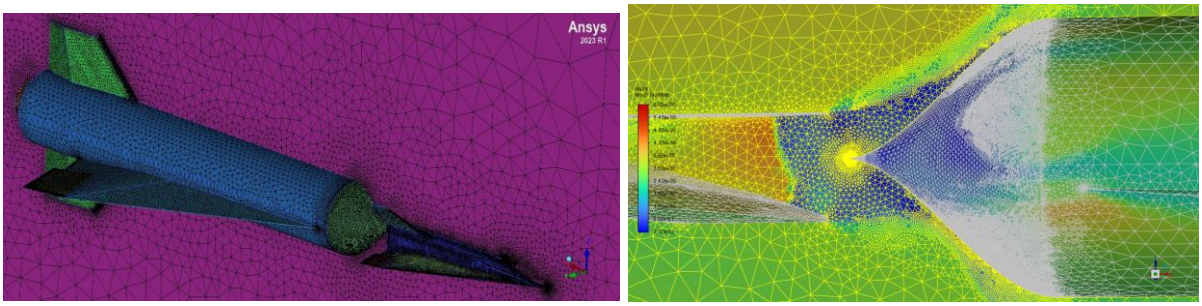

Figure 18 The full launch system grid (left) and an example of local adaptation on LV+SHEV grid for Mach=3.5 condition (right).

The full launch system aerodynamic coefficients as a function of Mach number and AoA are summarized in the following Figure **19** and Figure **20**.

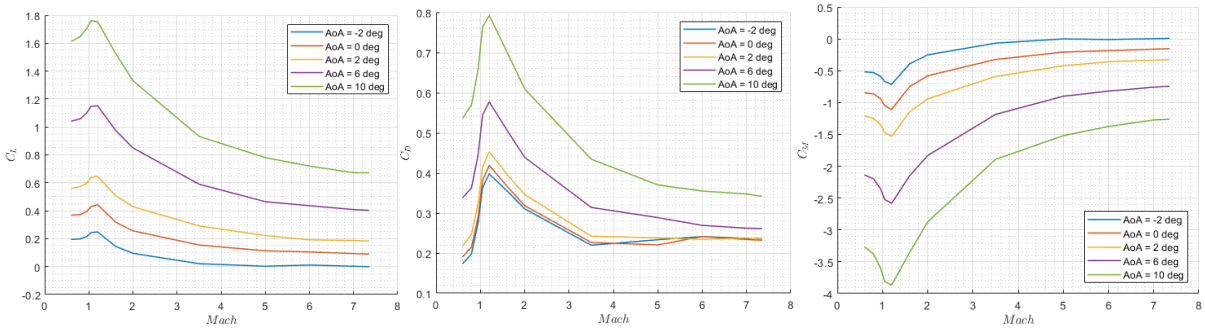

Figure 19 Aerodynamic coefficients as a function of Mach number, varying AoA.

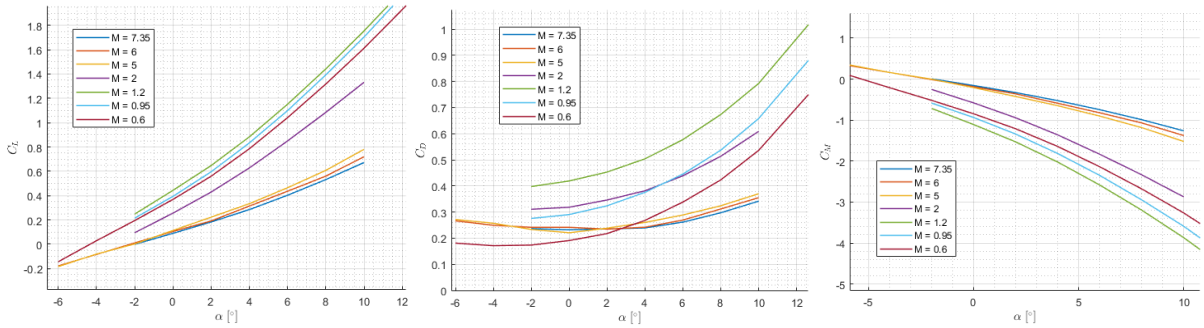

Figure 20 Aerodynamic coefficients as a function of AoA, varying Mach number.

It is important to notice that the pithing moment coefficients displayed in Figure 19 and in Figure 20 are relative to the SHEV nose (X = Y = Z = 0 m).
Then, assuming a linear variation of the Mach number with increasing altitude, it was possible to apply a viscous correction [10] to the drag coefficient (Figure 21).

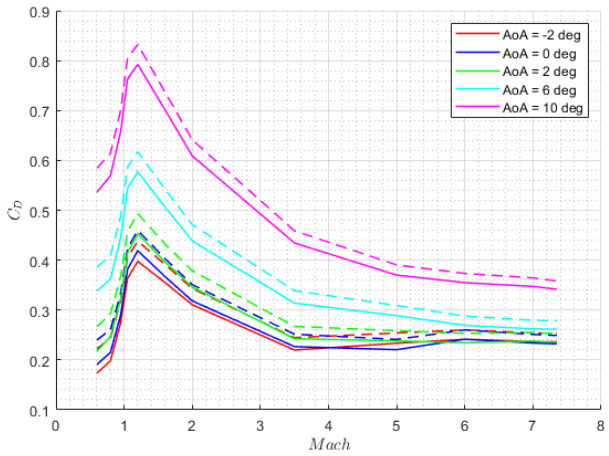

Figure 21 Comparison between inviscid drag coefficient (solid lines) and viscous drag coefficient (dashed line) as a function of Mach number.

From the CFD simulations carried out, it was observed that the presence of the LV behind the SHEV during the launch ascent trajectory causes a shock wave inside the nozzle of the SHEV itself. This effect is felt up to $M_\infty = 5$: once this Mach number is exceeded, the increase in pressure caused by the shaped cone is unable to rise back inside the nozzle, which is then able to eject out the shock.
This phenomenon is well described in the following Figure 22 for $M_\infty = 3.5$.

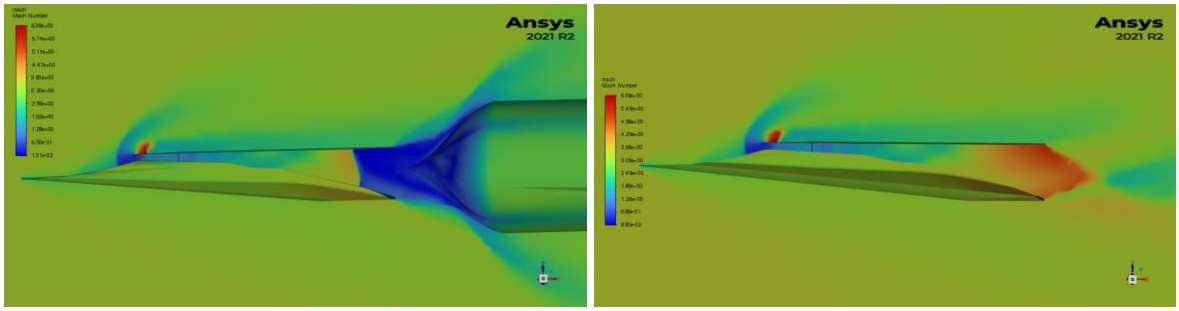

Figure 22 Mach number contours for the SHEV for $M_\infty = 3.5$ with LV (left) and without LV (right).

This effect can also be described by comparing the lumped aerodynamic coefficients of the SHEV, when the LV is present and when it is not present, see Figure 23. As expected, exceeding $M_\infty = 5$, they coincide: SHEV cannot be influenced by the presence of LV because the flow field is hyperbolic.

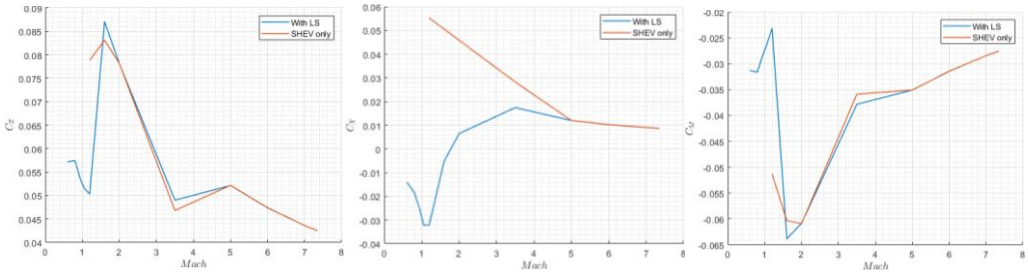

Figure 23 SHEV aerodynamic coefficients, with LV (blue line) and without LV (red line).

It is interesting to note that for low Mach numbers, the increase in pressure on the LV cone induces a negative drag coefficient (therefore thrusting) on the SHEV.
The wing of the LV (with its elevon) is an upscaled version of the SHEV's wing, thus allowing us to assume that the effect of the elevon of the LV is the same of the SHEV's elevon (previously calculated), of course properly scaled. In reality, this is not accurately valid due to energy loss through the curved shock on the shaped cone, but this hypothesis is reasonably acceptable at the moment.

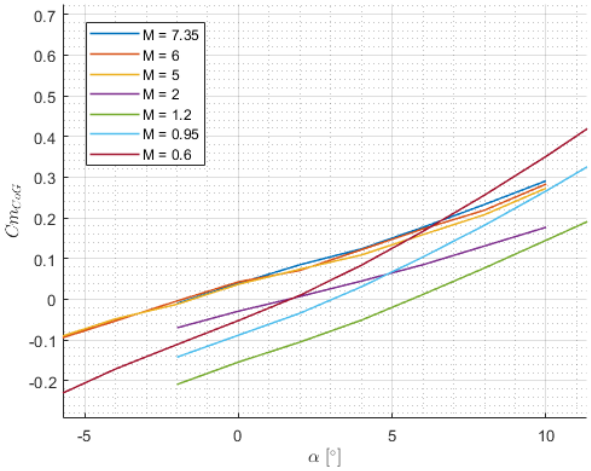

Figure 24 Pitching moment coefficient relative to CoG, as a function of AoA, varying Mach number.

Focusing back again on the aerodynamic coefficients, it is necessary to point out that the derivative of the pitching moment coefficient relative to the Centre of Gravity with respect to AoA would be important for the evaluation of the longitudinal stability and its static margin. In this case the CoG is varying over time due to the burning of the solid propellant of the booster Orion 50 ST [14]-[17], therefore it is not possible to evaluate the stability of the full launch system without an in-depth mission analysis. Despite this, for illustrative purposes, Figure 24 shows the C_M relative the CoG estimation at the moment of ignition of the solid propellant (x = 8.875 m behind the SHEV nose). The unstable nature of the full

launch system configuration clearly emerges due to the positive derivative of the pitching moment coefficient relative to the CoG. However, it must be taken into consideration that the slope of these curves will vary over time due to the shifting of the CoG.
Deeper analyses of both flight mechanics and aerodynamics will then follow, in order to verify the actual flyability of this configuration and evaluate possible changes in order to improve the stability.
However, it is possible to make some preliminary considerations in the trimmability of the full launch system. First of all, the effect of the LV elevon's deflection on global aerodynamic coefficients must be evaluated. The aerodynamic coefficients of the forces ($\Delta \boldsymbol{C_L}$ and $\Delta \boldsymbol{C_D}$), have been simply scaled by means of elevons wet surface ratio (this ratio is about 3.95):

$$\Delta C_{L_{LV}} = \Delta C_{L_{SHEV}} \cdot \frac{S_{LV}}{S_{SHEV}}$$
$$\Delta C_{D_{LV}} = \Delta C_{D_{SHEV}} \cdot \frac{S_{LV}}{S_{SHEV}}$$

Instead, the pitching moment coefficient has been scaled by means of the same surfaces' ratio, and also the ratio between the respective distance from the SHEV nose:

$$\Delta C_{M_{LV}} = \Delta C_{M_{SHEV}} \cdot \frac{S_{LV}}{S_{SHEV}} \cdot \frac{d_{LV}}{d_{SHEV}}$$

The distances "d" should be evaluated from the SHEV nose to each elevon's pressure centre: for simplicity purpose, the geometric centre of elevons have been considered (the ratio of distances is about 3).
Assuming the thrust trend of the Orion 50 ST [14]-[17] with a constant thrust vectoring angle (TV = 0°), a constant flight path angle (FPA = 12°), and the variation of the mass over the time, it is therefore possible to perform a preliminary check on flyability of the full launch system.
Figure 25 shows an indicative trend of AoA over time. For each Mach number, the AoA of trim is the one given by the elevon deflection that allows rotation around CoG (whose dynamics with respect to y axis is not considered in these analyses) and keeping the above said necessary angle of attack (AoA of trim). It must be considered that a constant FPA has been used in those equations. A non-constant FPA will cause a centrifugal force, changing the AoA of trim. For example, a pull-down manoeuvre (d(FPA)/dt<0) causes a centrifugal force that adds to the lift: for the trim, a minor AoA will be necessary.

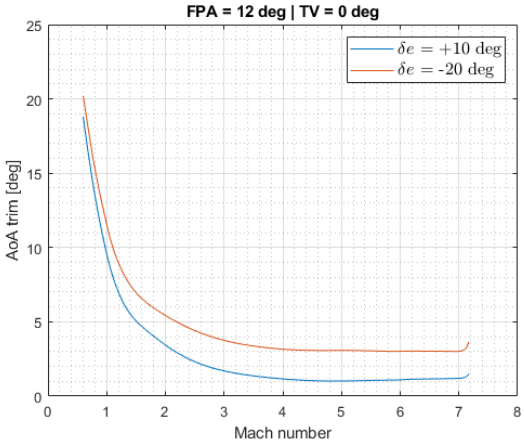

Figure 25 AoA trimming the full launch system for two different LV elevon deflections and TV = 0°.

Finally, it should be reasonable to make a preliminary and simplified assumption of FPA over time, in order to find a possible elevon deflection for each flight condition, as shown in Figure 26. Furthermore, the thrust vectoring angle is varying between -5° and 5°, allowing to find all the trimmed conditions.

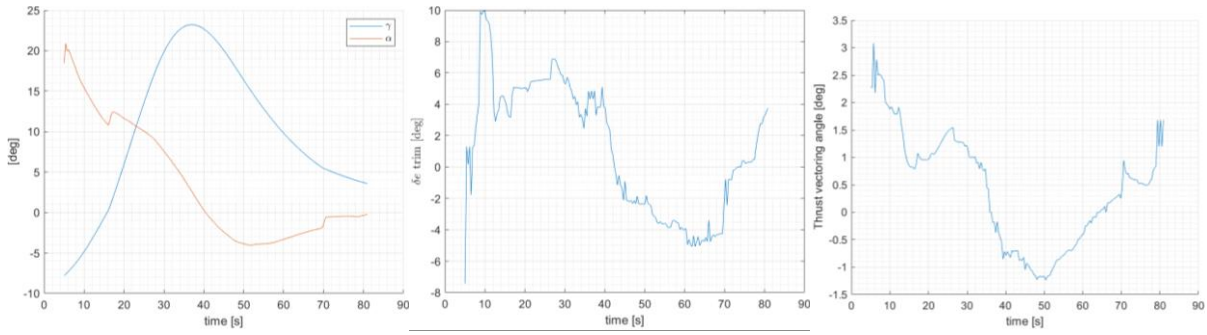

Figure 26 Trimming AoA, δ_e and TV for the assumed FPA.

To conclude, it can be stated that the LV+SHEV is trimmable but unstable, and consequently flyable by means of a very robust active control. However, some alternative configurations of Launch Vehicle LV are being evaluated that allow stable and trimmed flight in order to increase the reliability of the mission.

5. Conclusions

This paper reports the first results of the AEDB characterization for the SHEV vehicle obtained mainly from viscous and chemically reacting CFD simulations. The final AEDB will also take into account the experimental data results whose activity is going to start.
The main results can be summarized as follows:

- Positive aero-propulsive balance for two possible mission points, with a lower net thrust (as a percentage of total drag) at higher altitude due to the lower Reynolds number (higher viscous effects).
- Slight effect of altitude on Eulerian reactive simulations due to different asymptotic conditions of pressure and temperature (different hydrogen input conditions, chemical effect).
- Viscosity effect on engine performance: improved combustion efficiency due to better mixing, however viscous drag is added.
- Sensitivity conducted for chemical kinetics modelling of air-hydrogen combustion inside the internal flowpath (Intake-Combustor-Struts-Nozzle). The use of the multi-step "reduced-Jachimowsky chemical model" showed, in comparison to the mono-step, a reduction in gross thrust (Combustor and nozzle) of about 8% and in net thrust of about 11%.
- First version of the SHEV vehicle (demonstrator) aerodynamic database (AEDB) in the range of Mach = 7.35 – 2.00 delivered. The AEDB is based on CFD viscous calculations for the clean configuration and on CFD inviscid ones for the control surface effect. The AEDB has been provided to Flight Mechanics team for stability, trimmability and controllability analysis and trajectory calculations.
- The payload (SHEV + LV) has been characterized from the aerodynamic point of view showing the ability to perform the mission for what concerns trimmability all over the range of Mach. Alternative configurations of LV are being evaluated to improve stability and trimmability of the full system in order to increase the reliability of the mission.

Starting from the consolidated AEDB and trajectory analysis, next activities will focus on the maturation of the demonstrator design and on the selection of materials, together with the definition of test campaign on a scaled model.

Acknowledgements

The work has been funded by Italian Space Agency and CIRA ScpA in the frame of the agreement nr. 2022-13-HH.0 -F43D22000410005.

References

[1] J. Steelant, R. Varvill, C. Walton, S. Defoort, K. Hannemann, M. Marini, "Achievements Obtained for Sustained Hypersonic Flight within the LAPCAT-II Project", AIAA-2015-3677, 20th AIAA International Space Planes and Hypersonic Systems and Technologies Conference, July 06-09, 2015.

[2] E. Blanvillain, G. Gallic, "HIKARI: Paving the way towards High Speed Air Transport", AIAA-2015-3676, 20th AIAA International Space Planes and Hypersonic Systems and Technologies Conference, July 6-9, 2015.

[3] Mack A., Steelant J., Adirim H., Lentsch A., Marini M., Pilz N., "FAST20XX: Achievements on European Suborbital Space Flight", 7th European Symposium on Aerothermodynamics, Brugge, Belgium, May 2011.

[4] J. Steelant et al., "Achievements obtained within ATLLAS-II on Aero-Thermal Loaded Material Investigations for High-Speed Vehicles", 21st AIAA International Space Planes and Hypersonics Technologies Conference, 6-9 March 2017, China.

[5] J. Steelant et al., "Conceptual Design of the High-Speed Propelled Experimental Flight Test Vehicle HEXAFLY", AIAA-2015-3539, 20th AIAA International Space Planes and Hypersonic Systems and Technologies Conference, Glasgow, Scotland, U.K., July 6-9, 2015.

[6] G. Pezzella, M. Marini, M. Cicala, A. Vitale, T. Langener, J. Steelant, "Aerodynamic Characterization of HEXAFLY Scramjet Propelled Hypersonic Vehicle", AIAA-2014-2844, AIAA Aviation, 32nd AIAA Applied Aerodynamics Conference, 16-20 June 2014, Atlanta, GA, USA.

[7] Di Benedetto S., Di Donato M.P., Schettino A., Scigliano R., Nebula F., Morani G., Cristillo D., Marini M., Cardone S., Steelant J., Villace V., "The high-speed experimental flight test vehicle of HEXAFLY-INT: a multidisciplinary design",CEAS Space Journal, published online on 5 January 2021, DOI: 10.1007/s12567-020-00341-5.

[8] Viola N., Fusaro R., Saracoglu B., Schram C., Grewe V., Martinez J., Marini M., Hernandez S., Lammers K., Vincent A., Hauglustaine D., Liebhardt B., Linke F., Fureby C., "Main Challenges and Goals of the H2020 STRATOFLY Project", Aerotecnica Missili & Spazio (2021) 100:95–110, Published online: 29 May 2021, https://doi.org/10.1007/s42496-021-00082-6.

[9] Roncioni P., Vitagliano P. L., De Gregorio F., Pezzella G., Romano L., Paglia F., "Aerodynamic Appraisal of the VEGA-C Launcher", JSR-Journal of Spacecraft and Rockets, 24 April 2023, http://arc.aiaa.org | DOI: 10.2514/1.A35610.

[10] Viola N., Roncioni P., Gori O., Fusaro R., "Aerodynamic Characterization of Hypersonic Transportation Systems and Its Impact on Mission Analysis", MDPI-Energies, 16 June 2021, https://doi.org/10.3390/en14123580.

[11] S. Defoort, L. Serre, R. Grenon, Narmada, "ZEHST: Environmental challenges for hypersonic passenger transport", AIAA 2012-5873, 18th AIAA/3AF International Space Planes and Hypersonic Systems and Technologies Conference, September 2012.

[12] U. Mehta, M. Aftosmis, J. Bowles, S. Pandya, "SKYLON Aerodynamics and SABRE Plumes", AIAA 2015-3605, 20th AIAA International Space Planes and Hypersonic Systems and Technologies Conference, Glasgow, Scotland, U.K., July 6-9, 2015.

[13] Bahm C., Baumann E., Martin J., Bose D., Beck R.E., Strovers B., "The X-43A Hyper-X Mach 7 Flight 2 Guidance, Navigation, and Control Overview and Flight Test Results", AIAA/CIRA 13th International Space Planes and Hypersonic Systems and Technologies, May 2005, Capua, Italy. AIAA-2005-3275.

[14] Di Benedetto S., Marini M., Roncioni P., Vitale A., Vernillo P., Di Lorenzo G., Scigliano R., Cardone S., Albano M., Bertacin R., "The Scramjet Hypersonic Experimental Vehicle", HiSST-2024, The 3rd International Conference on High-Speed Vehicle Science Technology, 14 -19 April 2024, Busan, Korea.

[15] System engineering general requirements, ECSS-E-ST-10C.

[16] Technical requirements specification, ECSS-E-ST-10-06C.

[17] Northrop Grumman. Orion Motor Series Catalogue. *https://cdn.prd.ngc.agencyq.site/-/media/wp-content/uploads/Orion-Motor-Series.pdf*